Unbiased in vivo preclinical evaluation of anticancer drugs identifies effective therapy for the treatment of pancreatic adenocarcinoma

Olivera Grbovic-Huezo[a,b,c], Kenneth L. Pitter[b,d], Nicolas Lecomte[a,c], Joseph Saglimbeni[a], Gokce Askan[a,e], Matilda Holm[f], Jerry P. Melchor[a,c], Rohit Chandwani[g], Suhasini Joshi[h], Caj Haglund[f], Christine A. Iacobuzio-Donahue[a,c,e], Gabriela Chiosis[g,i], Tuomas Tammela[b,1], and Steven D. Leach[a,c,j,1]

[a]David M. Rubenstein Center for Pancreatic Cancer Research, Memorial Sloan Kettering Cancer Center, New York, NY 10065; [b]Cancer Biology & Genetics Program, Memorial Sloan Kettering Cancer Center, New York, NY 10065; [c]Human Oncology and Pathogenesis Program, Memorial Sloan Kettering Cancer Center, New York, NY 10065; [d]Department of Radiation Oncology, Memorial Sloan Kettering Cancer Center, New York, NY 10065; [e]Department of Pathology, Memorial Sloan Kettering Cancer Center, New York, NY 10065; [f]Translational Cancer Biology Research Program, University of Helsinki, 00014 Helsinki, Finland; [g]Department of Surgery, Weill Cornell Medicine, New York, NY 10065; [h]Chemical Biology Program, Memorial Sloan Kettering Cancer Center, New York, NY 10065; [i]Department of Medicine, Memorial Sloan Kettering Cancer Center, New York, NY 10065; and [j]Molecular and Systems Biology, Dartmouth Geisel School of Medicine and Norris Cotton Cancer Center, Lebanon, NH 03766

Edited by Ronald M. Evans, Salk Institute for Biological Studies, La Jolla, CA, and approved September 16, 2020 (received for review November 18, 2019)

Pancreatic ductal adenocarcinoma (PDAC) is typically diagnosed at an advanced stage, which limits surgical options and portends a dismal prognosis. Current oncologic PDAC therapies confer marginal benefit and, thus, a significant unmet clinical need exists for new therapeutic strategies. To identify effective PDAC therapies, we leveraged a syngeneic orthotopic PDAC transplant mouse model to perform a large-scale, in vivo screen of 16 single-agent and 41 two-drug targeted therapy combinations in mice. Among 57 drug conditions screened, combined inhibition of heat shock protein (Hsp)-90 and MEK was found to produce robust suppression of tumor growth, leading to an 80% increase in the survival of PDAC-bearing mice with no significant toxicity. Mechanistically, we observed that single-agent MEK inhibition led to compensatory activation of resistance pathways, including components of the PI3K/AKT/mTOR signaling axis, which was overcome with the addition of HSP90 inhibition. The combination of HSP90(i) + MEK(i) was also active in vitro in established human PDAC cell lines and in vivo in patient-derived organoid PDAC transplant models. These findings encourage the clinical development of HSP90(i) + MEK(i) combination therapy and highlight the power of clinically relevant in vivo model systems for identifying cancer therapies.

pancreatic cancer | PDAC | HSP90 | trametinib | MEK

Pancreatic ductal adenocarcinoma (PDAC) remains one of the most aggressive malignancies, with a 5-y survival rate of 10% (1). Traditional chemotherapies remain the standard of care for most PDAC patients despite providing incremental survival benefit (2, 3). Unlike for multiple other cancers, comprehensive efforts to characterize the transcriptional and mutational landscape of PDAC samples have failed to translate into significant therapeutic advances (4). Epidermal growth factor receptor (EGFR)-targeted therapy demonstrated a minor benefit, but collectively there have been no molecularly targeted agents demonstrating a meaningful response in late-phase clinical trials (5). As a consequence, pancreatic cancer patients continue to be in high need of effective therapeutic options. The relative lack of progress in PDAC compared to most other cancer types suggests novel approaches are required for identifying such therapies.

The failure to translate promising preclinical candidates into clinical advances can be partially explained by the inability of cell-based models to accurately predict anticancer activity in human trials (6). In vitro and subcutaneous (s.c.) transplant models are particularly limited in mimicking the tissue environment of primary pancreatic tumors, which is an important determinant of the therapeutic response (7). By contrast, autochthonous genetically engineered mouse models (GEMMs) generate tumors in the appropriate tissue context with a desmoplastic stroma similar to human PDAC (8). These models are based on the directed perturbation of *Kras* and *Trp53* by restricting Cre recombinase activity to pancreatic epithelial cells (*KPC* model). Although the *KPC* model is initiated during late embryogenesis, it recapitulates many key hallmarks of human PDAC and is a standard model in the field. However, broad adoption of *KPC* mice for high-throughput drug testing is hindered by the stochastic nature of PDAC development, the heterogeneity of tumors, and the large number of mice required for breeding.

To overcome these limitations, we designed an in vivo preclinical platform to identify and evaluate effective PDAC therapies for potential translation to the clinic. Here, we used a higher-throughput variant of the *KPC* model where PDAC tumors are generated by syngeneic orthotopic transplantation of

Significance

The clinical management of pancreatic cancer has not seen significant improvement in decades, in part because prediction of tumor drug sensitivity using in vitro assays has proven notoriously inaccurate in this disease. We performed a large-scale, unbiased in vivo screen of 57 different single agent and combination targeted therapies in an in vivo orthotopic mouse model. In this ambitious effort, we identified previously unsuspected synergy between HSP90 inhibition and MEK inhibition as effective combination therapy in this disease. The results underscore the utility of unbiased, in vivo drug screens in the identification of effective cancer therapies for evaluation in subsequent clinical trials.

Author contributions: O.G.-H. and S.D.L. designed research; O.G.-H., J.S., and M.H. performed research; N.L., J.P.M., S.J., C.H., C.A.I.-D., and G.C. contributed new reagents/analytic tools; O.G.-H., K.L.P., G.A., and R.C. analyzed data; and O.G.-H., K.L.P., T.T., and S.D.L. wrote the paper.

Competing interest statement: S.D.L. is member of scientific Advisory Board for Nybo Pharmaceuticals and a co-founder of Episteme Prognostics. Memorial Sloan Kettering Cancer Center holds the intellectual rights to this portfolio. Samus Therapeutics Inc, of which G.C. has partial ownership, and is a member of its board of directors, has licensed PU-H71. All other authors declare no competing interests.

This article is a PNAS Direct Submission.

[1]To whom correspondence may be addressed. Email: tammelat@mskcc.org or steven.d.leach@dartmouth.edu.

This article contains supporting information online at https://www.pnas.org/lookup/suppl/doi:10.1073/pnas.1920240117/-/DCSupplemental.

First published November 16, 2020.

PDAC cells into immunocompetent hosts. This allowed for large-scale, in vivo screening at an unprecedented scale. Screening a total of 57 single-agent and combination targeted therapies in over 450 mice, we identified combined inhibition of HSP90 and MEK as an effective and well-tolerated therapeutic strategy.

Results

Unbiased In Vivo Drug Screen Leads to Identification of Effective PDAC Therapies. In order to uncover effective therapeutic approaches for PDAC, we performed an in vivo preclinical screen of a panel of candidate therapies using a robust, reproducible, and disease-relevant mouse model of PDAC (Fig. 1*A*). We selected 57 strategies composed of monotherapies or drug combinations targeting signaling pathways known to be relevant in PDAC. To generate large cohorts of experimental animals we performed orthotopic transplantation of *KrasG12D* + *Trp53* mutant *KPC* (4662) cells into the pancreata of syngeneic C57BL/6 recipients as previously described (9, 10). Notably, the tumors generated by this method displayed moderately differentiated histology typical of autochthonous murine and human PDAC (Fig. 1*B*). After 10–14 d, mice were imaged using a high-resolution ultrasound imaging (HRUSI) to confirm the presence of tumors. Tumor-bearing mice were randomized into treatment groups ($n = 4$) at a time point when tumor volume was 100–200 mm^3 and enrolled in a 2-wk trial after which tumor volume was again assessed by HRUSI (Fig. 1*A*).

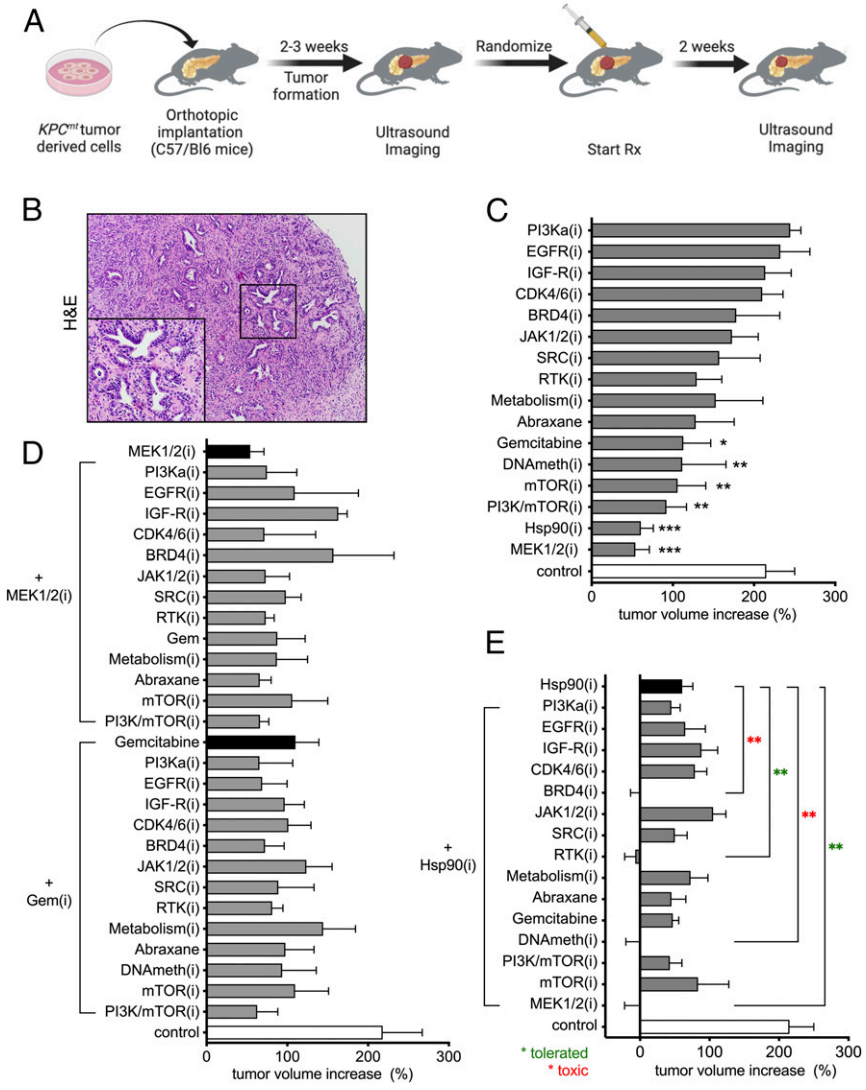

Fig. 1. In vivo drug screen identifies effective combinatorial therapeutic strategies for PDAC. (*A*) Schematic representation of in vivo drug screen design using syngeneic orthotopic KPC allografts. Two-week treatment was initiated when tumors were detected by HRUSI, at a time point when tumors were of 100–200 mm^3. (*B*) Hematoxylin and eosin staining of syngeneic PDAC tumors (magnification, 50×; *Inset*, 200×). (*C*) A waterfall representation of the average response of PDAC orthotopic transplants following a 2-wk treatment with the indicated monotherapies. Note that none of the drugs caused tumor regression (mean ± SEM; $n = 4$ per group; $^*P < 0.05$, $^{**}P < 0.01$; one-way ANOVA). (*D*) A waterfall representation of the average response of PDAC orthotopic transplants following a 2-wk treatment with GEM or the MEK1/2(i) trametinib, combined with 13 indicated therapies. Note that none of the drug combinations was significantly more effective than GEM or MEK1/2 (i) alone. ($n = 4$ per group; one-way ANOVA). (*E*) A waterfall representation of the average response of PDAC orthotopic transplants following 2 wk of treatment with HSP90(i) when combined with 15 indicated therapies. Note that four drug combinations showed enhanced efficacy and produced tumor regression. Among effective drug combinations, HSP90(i)+MEK1/2(i) and HSP90(i)+RTK(i) were well-tolerated (green asterisk) while HSP90(i)+DNAMeth(i) and HSP90(i)+BRD4(i) caused additive toxicity (see text, red asterisk) (mean ± SEM; $n = 4$ per group; $^{**}P < 0.01$; one-way ANOVA).

We first evaluated the effect of 16 different monotherapies on tumor growth. This panel included clinically approved chemotherapies (gemcitabine, nab-paclitaxel) as well as small molecule inhibitors (i) of signaling pathways, protein folding machinery, chromatin modifiers and metabolic regulators (Table 1). None of the 16 monotherapies elicited a notable tumor regression following 2 wk of drug administration using concentrations identified in previously published literature (Fig. 1*C*). However, several drugs, including gemcitabine (GEM), trametinib, a MAPK/ERK kinase (MEK)-1/2 inhibitor, and PU-H71, a heat-shock protein (HSP)-90 inhibitor with specificity for tumor HSP90 variants (11–14), significantly reduced tumor growth when compared to control.

Encouraged by these findings, we next sought to identify two-drug combination that could further sensitize tumors to the antiproliferative effect observed with GEM, or with either of the most active targeted monotherapies, trametinib and PU-H71. In a similar experimental design, four tumor bearing mice per group were treated for 2 wk with a combination of two agents using the same dose and schedule as in the single-agent trials. As in the monotherapy study, mouse weight was monitored daily to assess systemic toxicity of the drug combinations. The combination of the MEK1/2 inhibitor trametinib with 13 different compounds did not lead to an improved antitumor effect over trametinib alone (Fig. 1 *D*, *Upper*). Similarly, no significant additional tumor growth inhibition was achieved with the same panel of drugs when combined with GEM chemotherapy (Fig. 1 *D*, *Lower*). In contrast, we identified four compounds that increased the effectiveness of the HSP90 inhibitor, PU-H71 (Fig. 1*E*): the MEK1/2 inhibitor trametinib (T), the broad-spectrum receptor tyrosine kinase (RTK) inhibitor sunitinib, the DNA methyltransferase DNMT inhibitor 5-aza-2′-deoxycytidine (decitabine), and the bromodomain-containing protein (BRD)-4(i) JQ1. Each of these compounds elicited a significantly more effective inhibition of tumor growth when combined with PU-H71 than either drug alone. However, treatment of mice with either HSP90(i) + DNMT(i) or HSP90(i) + BRD4(i) combinations induced a significant body weight loss over the 2-wk treatment period, indicative of compounded drug toxicity. No apparent additive drug toxicity was observed in groups of mice treated with *PU-H71* + T or *PU-H71* + broad-spectrum RTK(i) (*SI Appendix*, Fig. S1).

Combined Administration of PU-H71 and Trametinib Significantly Increases Survival of PDAC Tumor-Bearing Mice. We next initiated a long-term drug efficacy and tolerability study to further evaluate the trametinib + PU-H71 combination (Fig. 2). Cohorts of PDAC-bearing mice produced by orthotopic transplantation of *KPC* cells were enrolled in the experiment upon detection of pancreatic tumors by HRUSI (as in the initial screen), and tumor volume was measured weekly (Fig. 2*A*). In concordance with our initial single agent screen above, administration of trametinib (T) or PU-H71 (P) alone initially delayed tumor growth when compared to the vehicle control group (Fig. 2*B*). However, this effect was not durable and single agent-treated tumors eventually reached a size comparable to vehicle control. Consistent with this, trametinib treatment alone did not significantly improve overall survival of PDAC-bearing mice compared to vehicle-treated mice (52 d vs. 46 d, $P = 0.3136$), whereas PU-H71 monotherapy produced a modest survival advantage (63 d vs. 46 d, $^{**}P < 0.0014$, Fig. 2*C*). In contrast, the T/P combination was highly effective at impairing tumor growth and produced a significant survival benefit, extending the median survival of mice by 1.8-fold over control (83 d vs. 46 d, $P < 0.001$, Fig. 2*C*).

To further investigate the biological effects of T/P combination therapy in PDAC tissues, we performed histological analysis of treated tumors compared to vehicle control tumors. Cancer cell proliferation, as determined by Ki67 positivity, was significantly reduced in tumor tissues of mice treated with T/P combination, but not with either drug alone (Fig. 2*D*). We also detected lower pERK immunosignal in tumor tissues treated with T and T/P combination but not in tumors treated with PU-H71 alone (Fig. 2*E*). Moreover, treatment with PU-H71 with trametinib led to an increase in apoptosis, as assessed by terminal deoxynucleotidyl transferase dUTP nick-end labeling (TUNEL) (Fig. 2*F*).

Targeting HSP90 Suppresses Feedback Pathway Reactivation and Enhances the Activity of MEK-Targeted Therapy. Having confirmed the durable efficacy and tolerability of combining trametinib and PU-H71 in vivo, we next sought to explore potential cancer cell-autonomous mechanistic effects of the combination by in vitro assays using the *KPC* (4662) cells. As expected, cell growth was markedly inhibited after a 72-h exposure to each inhibitor ($IC_{50} = 32.4$ nM for trametinib and $IC_{50} = 286$ nM for PU-H71) and was further inhibited with the T/P drug combination,

Table 1. Targeted and nontargeted drugs used for in vivo drug screen

Target	Inhibitor	Dose, mg/kg	Schedule	Route	Solvent
CDK4/6	Palbociclib	50	QD	p.o.	Sodium lactate buffer (50 mM, pH 4.0)
Microtubule inhibitor	Abraxane	30	1x/week	i.p.	Saline
PI3K	Alpelisib	50	QD	i.p.	1% (wt/vol) Carboxymethylcellulose (CMC)+0.5% (wt/vol) Tween 80
RTK	Sunitinib	40	QD	p.o.	0.5% Carboxy-methylcellulose, ph3.5
JAK1/2	Ruxolitinib	60	QD	p.o.	0.1% Tween 80
HSP90	PU-H71	75	3x/week	p.o.	Phosphate buffer
EGFR	Erlotinib	25	QD	p.o.	0.5% methylcellulose
mTOR	Temsirolimus	10	QD	i.p.	4% ETOH+2% Tween 80+5% PEG 400
PI3K/mTOR	NVP-BEZ235	50	3x/week	p.o.	NMP/polyethylene glycol 300 (10/90, vol/vol)
IGF-R	BMS-754807	25	QD	p.o.	30% PEG400+0.5% Tween 80+5% Propylene glycol
Metabolism	Phenformin	100	QD	p.o.	Water
DNA	Gemcitabine	400	1x/week	i.p.	Saline
MEK1/2	Trametinib	2	QD	p.o.	0.5% HPMC+0.2%Tween 80
Src	Dasatinib	30	BID	p.o.	80 mM sodium citrate pH 3.1
DNA methyl transferase	5-Azacytidine (Decitabine)	3	QD	i.p.	Saline
BET bromodomain	(+)-JQ-1	50	QD	p.o.	10% 2-Hydroxypropyl-beta-cyclodextrin

BID, two times per day; i.p., intraperitoneal; p.o., per oral gavage; QD, every day.

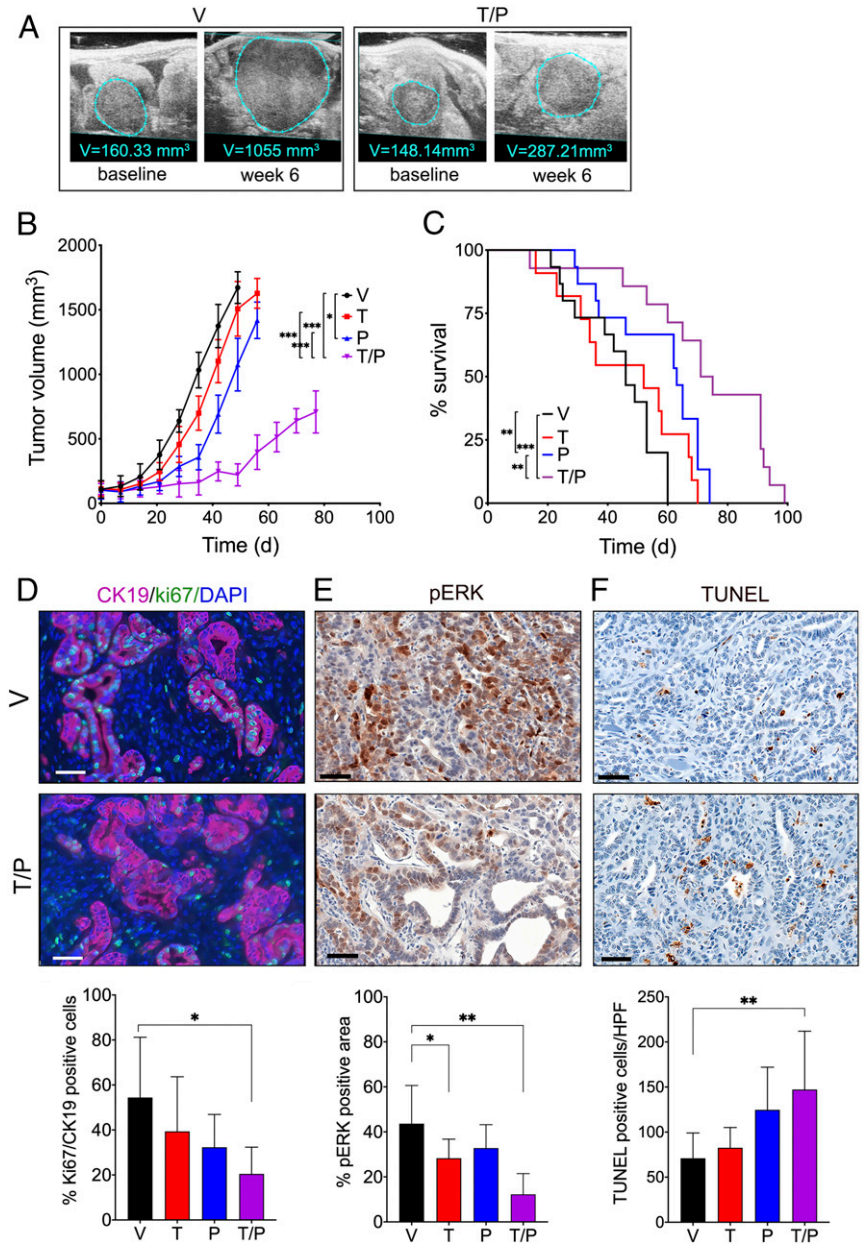

Fig. 2. HSP90+MEK inhibitor combination therapy significantly extends survival. (*A*) Representative images of the changes in orthotopic tumor volumes in mice treated with vehicle or T/P combination therapy for 6 wk as recorded by HRUSI. Tumor outline is indicated by blue line. (*B*) Tumor volumes of mice bearing PDAC tumors treated with vehicle ("V"), trametinib ("T", 2 mg/kg per day), PU-H71 ("P", 75 mg/kg per day), or T/P for indicated times (mean ± SEM; $n > 8$ per group; $^{*}P < 0.05$, $^{**}P < 0.01$, $^{***}P < 0.001$; two-way ANOVA); (*C*) Kaplan–Meier survival curve of mice bearing PDAC tumors treated as described in *AA* ($n > 8$ per group; $^{**}P < 0.01$; $^{***}P < 0.001$; log-rank test). (*D–F*(*D–F*) Quantification of proliferating Ki67/CK19+ cells (*D*), pERK+ cells (*E*), and dead/dying TUNEL+ cells (*F*) in PDAC tumors treated for 8 wk with vehicle or the T/P combination as described in *AA* (mean ± SEM; $n = 5$ per group; $^{*}P < 0.05$, $^{**}P < 0.01$; unpaired two-tailed *t* test). Representative immunohistochemical or immunofluorescence stainings are shown. (Scale bars, 50 μm.)

indicative of synergistic effect with the two-drug combination (Fig. 3*A*). This effect was observed using several other HSP90 inhibitors, suggesting that the synergistic effects of HSP90 and MEK inhibition were not due to off-target effects of PU-H71 (*SI Appendix*, Fig. S2).

To further dissect the molecular mechanisms underlying the increased effectiveness observed with the MEK1/2(i) + HSP90(i) combination, we subjected whole-cell lysates of *KPC* cells, treated with DMSO vehicle (V), trametinib (T), PU-H71 (P), or the T/P combination for 24 h to reverse phase protein arrays (RPPAs) (Fig. 3*B*). Consistent with the decreased growth observed in vitro, the two-drug combination significantly down-regulated essential cell cycle checkpoint and proliferation proteins, such as RAD51, CHK-1, pCDC2, and pRb. Levels of the proapoptotic proteins PDCD4, BIM, and RIP were increased by monotherapy treatment and were further elevated with the T/P combination (Fig. 3*B*), consistent with the higher cytotoxic activity of T/P compared to either agent alone. Trametinib alone however, uniquely induced up-regulation of the RTK/AKT/mTOR signaling axis as demonstrated by increased levels of Heregulin (ligand for ErbB3/4 kinase), pAKT, mTOR, pNDRG1, and E2F1 (Fig. 3*B*). Conversely, PU-H71 alone

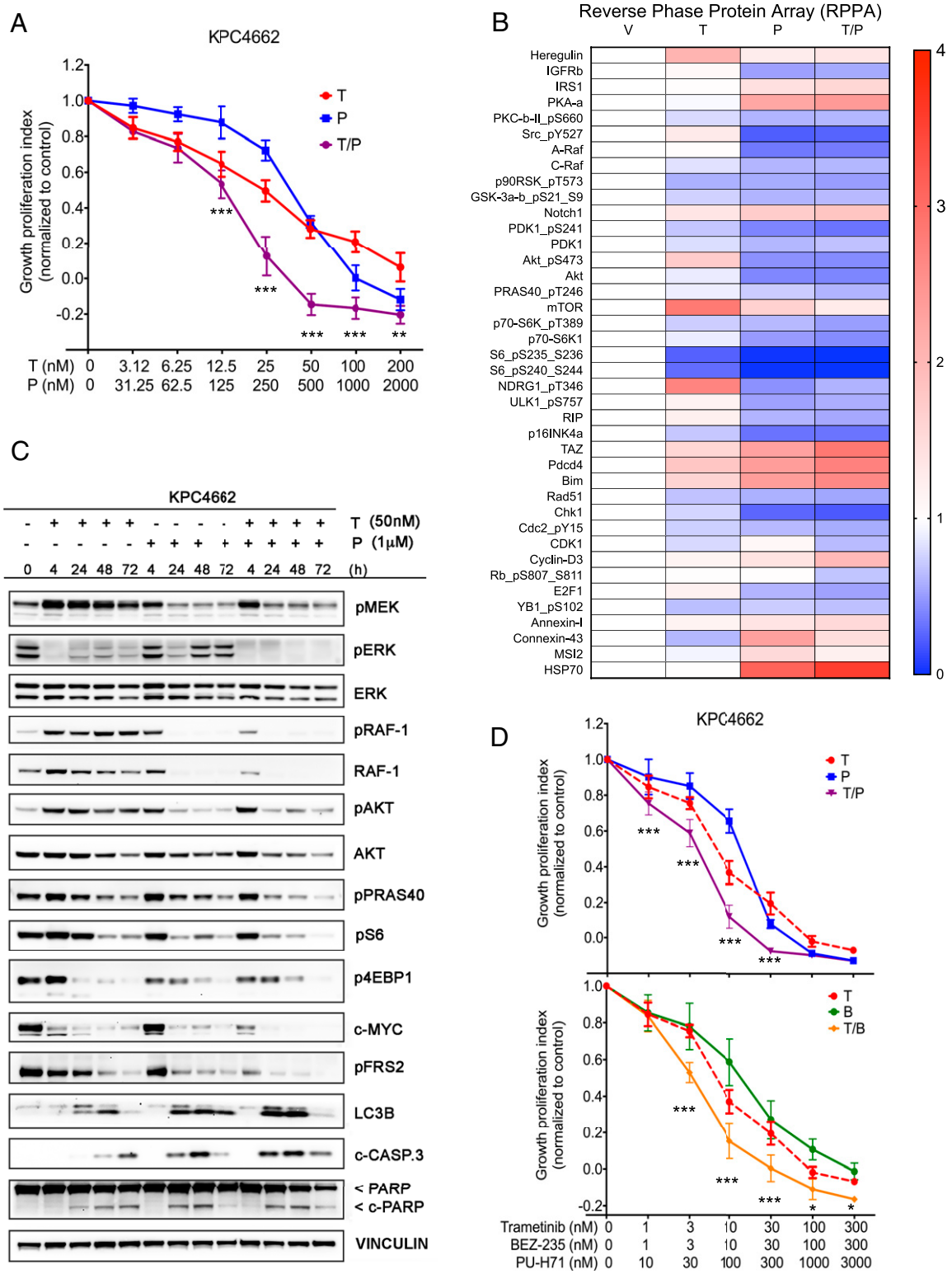

Fig. 3. MEK1/2(i) and HSP90(i) synergize to suppress the PI3K/AKT/mTOR and MAPK signaling pathways. (*A*) Cell growth analysis of KPC4662 cells treated for 3 d with vehicle (V) and increasing concentrations of trametinib (T), PU-H71 (P), or T/P. Cell viability was determined using the Cell Titer Glo (CTG) assay and plotted as percentage of control. Representative results from three independent experiments are shown ($n = 6$, mean ± SEM, two-way ANOVA). (*B*) Heat map of protein expression in KPC4662 cells following 24 h treatment with trametinib (50 nM) and/or PU-H71 (1 μM) as assessed by RPPA. Data presented as mean of three biological replicates for 42 significantly differentially expressed proteins normalized to control (>1.5-fold change, $P < 0.05$, one-way ANOVA). (*C*) Representative Western blotting analysis of protein expression in KPC4662 cells following 4, 24, 48, and 72 h treatment with DMSO, trametinib (50 nM), and/or PU-H71 (1 μM). Note simultaneous and sustained inhibition of MAPK and PI3K/AKT/mTOR signaling pathways with the two-drug combination, unlike with either agent alone. Also note increase in cleaved PARP and cleaved caspase-3 levels with the T/P combination. (*D*) Cell growth analysis of KPC4662 cells treated for 3 d with increasing concentrations of trametinib (T), PU-H71 (P), T/P combination, BEZ-235 (B), and (T/B) combo. Cell viability was determined using the CTG assay and plotted as percentage of control. Note similar level of growth inhibition obtained with both T/P and T/B combinations.

lowered levels of pAKT and total AKT, as well their upstream activator IGFR. In addition, PU-H71 treatment lowered levels of pSRC, A-Raf, and Raf-1 (C-Raf) signaling, which are known to drive Ras/MEK/ERK pathway activity. Importantly, the addition of HSP90 inhibition overcame the compensatory increase in PI3K/mTOR pathway observed with trametinib alone (Fig. 3*B*). In similar fashion, where single agents lowered levels of p90RSK, p70S6 kinase, and pS6 that are essential for protein translation, the response to the T/P combination was more robust (Fig. 3*B*).

The changes in activity of signaling pathways observed by RPPA were validated and further complemented by Western blotting of *KPC* cells (Fig. 3*C*). Trametinib alone, as expected, effectively inhibited ERK activity already after 4 h of drug exposure. However, by 24 h and throughout longer exposure to the drug, we detected a rebound in pERK that correlated with a strong and durable increase in levels of pMEK and pRAF-1, consistent with previously described elements of ERK pathway reactivation (15, 16). Additionally, trametinib treatment resulted in compensatory activation of the PI3K/AKT/mTOR pathway as assessed by AKT, PRAS40, S6, and 4EBP1 phosphorylation (Fig. 3*C*). PU-H71 treatment reduced activity and total levels of the well-established HSP90 client proteins RAF-1 and AKT (17, 18), resulting in a transient reduction of pERK levels at 24 h that rebounded at later time points. However, T/P-treated cells demonstrated sustained and durable inhibition of pERK levels without detectable evidence of rebounding ERK activity or increasing pMEK levels over time. The T/P combination produced further inhibition of downstream PI3K/mTOR pathway effectors, such as PRAS40, S6, and 4EBP1, effective inhibition of c-MYC, and apoptosis induction over time, as shown by an increase in cleaved poly-ADP ribose polymerase (c-PARP) and cleaved Caspase-3 (c-CASP3) (Fig. 3*C*).

In addition to the PI3K/mTOR pathway, the addition of HSP90 inhibition to MEK inhibition was also associated with more effective inhibition of fibroblast growth factor (FGF) receptor substrate 2 (FRS2), known to link FGF-receptor activation to the Ras/MAPK signaling pathway and also associated with resistance to MAPK inhibition (16). An alternative response to MAPK inhibition that has been described in PDAC is the induction of autophagy (19). Using the autophagy marker LC3B, we observed induction of autophagy in response to single inhibition of MEK and HSP90, and this induction was increased by dual inhibition (Fig. 3*C*). This would suggest that HSP90 inhibition does not sensitize PDAC to MEK inhibition via suppression of autophagy.

Although HSP90(i) can target multiple kinase clients, these data suggest that HSP90 inhibition contributes synergistically to MEK inhibition in part by reducing RAF-1 and AKT protein levels, thereby impairing respectively the RAF/MEK/ERK and PI3K/AKT/mTOR signaling axeses and rendering cells more sensitive to trametinib. Similar effects were observed using 7-dimethylaminoethylamino-17-demethoxygeldanamycin, an alternative small molecule HSP90 inhibitor (*SI Appendix*, Fig. S3). We next hypothesized that if PU-H71–mediated inhibition of PI3K/AKT/mTOR signaling has a major role in sensitizing cells to trametinib, substitution of PU-H71 with the dual PI3K/mTOR inhibitor BEZ-235 should produce a comparable effect. Indeed, we found that both two-drug combinations were superior to either single agent in inhibiting growth of *KPC* cells over 72 h (Fig. 3*D*). Collectively, these in vitro data are consistent with the enhanced therapeutic efficacy observed in our in vivo screen and provide a potential mechanistic rationale for the observed synergistic effect, i.e., the HSP90i-mediated suppression of trametinib-induced resistance pathways, including PI3K/AKT/mTOR signaling.

Dual MEK and HSP90 Inhibition Has Activity in Established Human PDAC Cell Lines and in Patient-Derived Organoid Models. To expand on the potential clinical relevance of these findings, we next assayed the combination of trametinib and PU-H71 in established human PDAC cell lines. Similar to the murine cell line *KPC*4662, human MiaPaca2 cells treated with single agent MEK(i) or HSP-90(i) had impaired cell growth (IC_{50} =19.4 nM for trametinib and IC_{50} = 121.5 nM for PU-H71) that was further decreased with the T/P combination (Fig. 4*A*). Similar effects were seen other seven human PDAC cell lines (*SI Appendix*, Fig. S4). Quantifying the potential pharmacologic synergy of trametinib and PU-H71 in eight established human PDAC cell lines (20), we observed synergy of the two drugs in half of the cell lines and an additive effect in the other half (Fig. 4*B*). The epithelial vs. mesenchymal morphology of the cell lines (21) did not appear to predict synergistic vs. additive effects on cell growth in response to the T/P combination. Interestingly, evaluating the genetic profiles of the cell lines (22) revealed copy number changes in *AKT2* and *AKT3* in the three cell lines that had the least degree of synergy with the T/P combination (*SI Appendix*, Fig. S5). However, a more in-depth investigation of molecular predictors of synergy and response of pancreatic tumors to these inhibitors and their combination is required to establish causality of the genomic patterns.

At the cell signaling level, trametinib treated MiaPaca2 cells had an initial decrease of pERK levels that lessened over 48–72 h and was associated with increased pMEK and pRAF levels (Fig. 4*C*). We did not detect a compensatory trametinib-induced increase in pAKT levels by 72 h, although this effect has previously been observed after longer treatment periods in this cell line (16). As seen in the murine *KPC* cells, PU-H71 treatment led to down-regulation of pRAF and effectors of the AKT/mTOR signaling axis, as well as partial reduction of pERK (Fig. 4*C*). The combination treatment lead to consistent and robust down-regulation of both signaling pathways, associated with decreased c-MYC levels and increased cell death as detected by increased cleaved PARP and cleaved Caspase-3.

Although the results described above draw important parallels between murine and human PDAC cells, two-dimensional (2D) cell culture conditions have well-documented pitfalls for developing viable clinical strategies, in particular for PDAC (7). To further validate the potential clinical utility of dual MEK and HSP90 inhibition, we next turned to patient-derived organoid models of PDAC. These models have recently emerged as highly effective preclinical tools for predicting efficacy of both established and investigational anticancer therapeutics (23–26). Two patient-derived organoid lines from distinct patients were established in Matrigel culture (23), engineered to constitutively express firefly luciferase, and orthotopically transplanted into immunodeficient NOD.Cg-*Prkdc*^{scid} *Il2rg*^{tm1Wjl}/SzJ (NSG) mice. Following tumor engraftment and baseline bioluminescence imaging, mice were randomized and treated with vehicle, trametinib, PU-H71, or T/P combination according to the same dosing scheme as the *KPC* model (Fig. 1*A*). After 2 wk of treatment, tumor growth across all mice receiving T/P combination was reduced by 79% comparing to vehicle-treated mice (Fig. 4*D* and *SI Appendix*, Fig. S6, mean fold change ± SD, 0.58 ± 0.3 for TP vs. 2.82 ± 1.45 for V; $P = 0.0043$), whereas change in BLI signal in mice receiving either monotherapy did not reach significance (mean fold change ± SD for T: 2.42 ± 0.59, $P = 0.53$, and for P: 2.088 ± 1.211, $P = 0.31$). These data demonstrate robust antitumor activity of dual MEK and HSP90 inhibition in vivo in a clinically relevant patient-derived model.

To assess the safety of dual MEK and HSP90 inhibition, blood was collected from tumor-bearing NSG mice for hematological and biochemical analyses. We observed no evidence of hematological, renal, or liver dysfunction in any of the experimental groups (*SI Appendix*, Fig. S7*A*). Blood glucose levels were

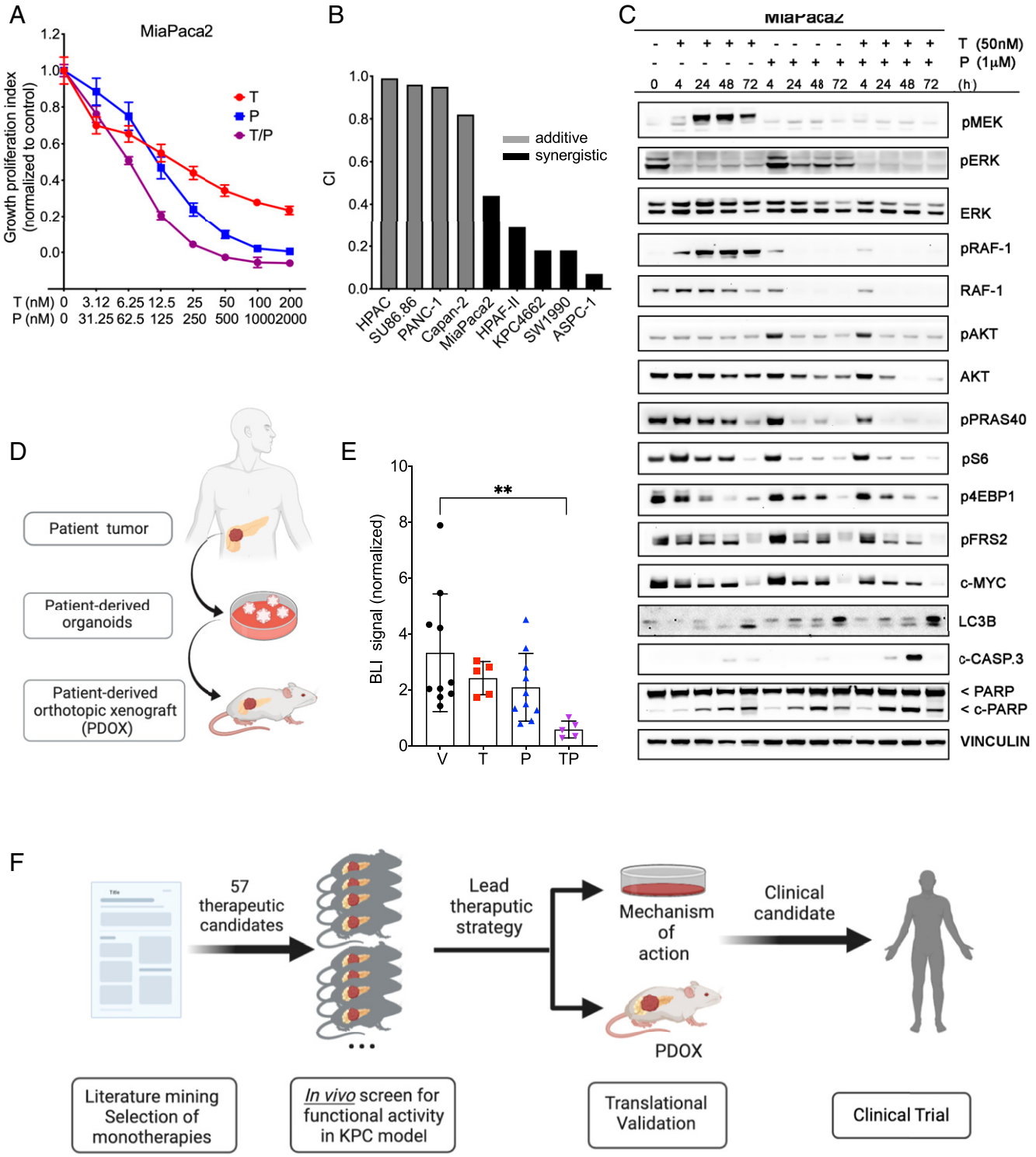

Fig. 4. Trametinib and PU-H71 have antitumor activity in human PDAC models in vitro and in vivo. (*A*) Cell growth analysis of MiaPaca2 cells treated for 3 d with vehicle (DMSO) and increasing concentrations of trametinib (T), PU-H71 (P), or T/P. Cell viability was determined using the CTG assay and plotted as percentage of control. Representative results from three independent experiments are shown ($n = 6$, mean ± SEM, two-way ANOVA). (*B*) Drug synergism calculations for eight established human PDAC cell lines. Combination index (CI) < 0.75 indicates synergism, CI 0.75–1.25 indicates additive effects, and CI > 1.25 indicates antagonism. (*C*) Representative Western blotting of protein levels in MiaPaca2 cells following 4, 24, 48, and 72 h treatment with DMSO, trametinib (50 nM), and/or PU-H71 (1 μM). Note simultaneous and sustained inhibition of two major signaling pathways, MAPK and PI3K/AKT/mTOR, with the two-drug combination, unlike with either agent alone. Also note increase in cleaved PARP and cleaved caspase-3 levels in response to the T/P combination. (*D*) Schematic depicting generation of human patient-derived organoid (HPDO) lines. (*E*) Fold change in bioluminescence in NSG mice bearing orthotopic HPDO xenografts treated with vehicle, trametinib (2 mg/kg per day), PU-H71 (75 mg/kg per day) at day 14 normalized to the day before starting treatment (6 wk posttransplant) (mean ± SEM; $n = 5$ per group, $^{**}P < 0.01$; one-way ANOVA). (*F*) Schematic outlining in vivo orthotopic transplant drug screening approach to identify novel candidate therapies.

normal and comparable in all groups, indicating no overt pancreatic endocrine dysfunction. We found a statistically significant increase in levels of aspartate aminotransferase (AST) levels, alanine transaminase (ALT), and alkaline phosphatase (ALP) enzymes in T/P-treated animals. On average AST and ALT levels were 1.6-fold higher in T/P-treated animals, consistent with a grade 1 transaminitis in two of five treated animals. On average, ALP levels were increased 1.7-fold, with no animals exhibiting grade 1 toxicity (twofold increase from normal levels). Additionally, neither immunodeficient nor immunocompetent tumor-bearing mice exhibited a significant change in weight during treatment (*SI Appendix*, Fig. S7*B*).

Discussion

Identification of novel therapeutic strategies in pancreatic cancer remains a major clinical challenge. In this study, we sought to identify well-tolerated synergistic therapeutic strategies in a highly disease-relevant in vivo preclinical model. Past studies have relied extensively on in vitro and s.c. transplant models, which although amenable to relatively high throughput, have limitations which have hindered the ability to translate preclinical findings into clinical advances (7, 27–29). Here, we describe a stepwise in vivo preclinical drug screening approach leveraging an orthotopic genetically engineered mouse model of PDAC. Using this approach, we were able to accomplish large-scale screening of 57 different single and combination drug therapies in over 400 mice. In so doing, we identified dual inhibition of MEK and HSP90 as a potent synergistic therapeutic strategy. This combination resulted in prolonged survival of PDAC-bearing mice and was associated with decreased cancer cell proliferation and increased cell death. We further identified a potential biochemical rationale for the observed synergy: Simultaneous HSP90 and MEK inhibition suppressed compensatory resistance pathways to MEK inhibition, including reactivation of the PI3K/ATK/mTOR, MYC, and FGF receptor pathways. Importantly, combining MEK and HSP90 inhibition demonstrated in vitro activity in a panel of established human PDAC cell lines and potently suppressed growth of orthotopically transplanted human patient-derived PDAC organoid lines with limited normal tissue toxicity, suggesting that this therapeutic combination may be active and well tolerated in humans. Collectively, these data provide a rationale for unbiased in vivo drug discovery strategies and identify dual MEK + HSP90 inhibition as an attractive therapeutic combination in PDAC.

The most common oncogenic driver in PDAC is mutationally activated KRAS, detected in over 94% of PDAC patients (30). Thus far, therapeutic strategies to inhibit mutant KRAS variants and its effector pathways, such as the MAPK/ERK and PI3K/AKT signaling axes, have failed in PDAC, in part due to the presence of multiple compensatory and coactivated signaling pathways that contribute to cell proliferation and survival (31). The MEK inhibitor trametinib is approved by the Food and Drug Administration for the treatment of melanoma and NSCLC harboring BRAF-V600E mutations. Yet, its single-agent activity has been limited due to rapidly acquired resistance (32–34). In PDAC specifically, several resistance mechanisms to MEK inhibition have been described, including induction of c-MYC, FGFR signaling, ERK5 signaling, AKT signaling, or RAF-1 (15, 16, 19, 35, 36). Our results demonstrate that one mechanism underlying the synergy between the HSP90 and MEK inhibitors lies with the ability of the HSP90 inhibitor to suppress compensatory activation of RAF-1 and the PI3K/mTOR/AKT pathways. Additionally, we also observe synergistic suppression of the FGFR signaling pathway and c-MYC protein levels, suggesting that multiple compensatory pathways may be impacted.

HSP90 functions as a chaperone protein for a number of client proteins critical for the growth and survival of cancer cells (37), and its elevated expression is correlated with poor prognosis in PDAC and in multiple other cancers (38). The link between HSP90 inhibition and suppression of PI3K/AKT/mTOR signaling has been previously reported in a number of solid and hematological malignancies, and our results support these findings (17, 39, 40). In addition, HSP90 is shown to be critical for B-RAF or RAF-1–induced MEK activation (18). Our data suggest that HSP90 inhibition sensitizes PDAC tumors to MEK inhibition by effectively suppressing multiple adaptive resistance mechanisms, including the RAF-1 and AKT signaling pathways. Concurrent pharmacologic targeting of RAF/MEK/ERK and PI3K/AKT/mTOR pathways in KRAS-driven cancer models has been reported, but clinically this strategy has been limited by additive toxicity (41). Importantly, our study demonstrates a significant survival benefit and minimal combined toxicities using dual MEK/HSP90 inhibition in PDAC-bearing mice.

Our goal was to develop an improved preclinical drug screening platform based on advanced in vivo model systems with high translational utility. While these results are promising, there remain potential translational hurdles to address. Although orthotopically transplanted *KPC* cell lines still exhibit significant collagen deposition (42), they are less desmoplastic than the human tumors they mimic. The desmoplastic stroma plays an important role in the therapeutic resistance of PDAC (43) and may serve as a potential barrier to advancing MEK/HSP90 inhibition. Additionally, despite the impressive survival advantage offered by dual MEK/HSP90 inhibition, tumors did eventually progress on treatment and future studies are needed to identify mechanisms of resistance.

Collectively, our results provide a preclinical and translational rationale for combining MEK and HSP90 inhibitors in pancreatic cancer therapy. Although careful attention to systemic toxicities will be required for the clinical implementation of these findings, our in vivo data suggests that simultaneous targeting of MEK and HSP90 pathways will be well-tolerated and effective in abolishing multiple intrinsic and adaptive mechanisms of resistance previously observed when targeting KRAS-driven pathways in PDAC. This work highlights the potential of large-scale preclinical in vivo drug screening for uncovering effective therapeutic strategies for PDAC.

Materials and Methods

Murine *KPC*4662 PDAC cells were obtained from Robert Vonderheide, Abramson Cancer Center, Perelman School of Medicine, University of Pennsylvania, Philadelphia, PA, generated from a *Kras*$^{LSL\text{-}G12D/+}$, *Trp53*$^{LSL\text{-}R172H/+}$, *Pdx1-Cre* mouse in the C57black/6j genetic background (10). Human PDAC lines MiaPaCa-2, Panc-1, Capan-2, AsPC1, HPAF, HPAC-1, SW1990, SU.86.86 were obtained from the American Type Culture Collection. Primary patient-derived PDAC organoids 3 and 83 were generated at Memorial Sloan Kettering Cancer Center (MSKCC) using primary patient samples from tumor resection under Institutional Review Boards approval (MSKCC IRB 15-149 or 06-107). Detailed information on condition media for maintenance of human organoids, inhibitors and other reagents, experimental design of in vivo animal studies, cell viability assay, RPPA, Western blotting, histology, and immunohistochemistry are given in detailed descriptions in *SI Appendix*, *SI Appendix, Materials and Methods*.

Data Availability. All study data are included in the article and supporting information.

ACKNOWLEDGMENTS. This work was supported by a Lustgarten Foundation Research Investigator Award (to S.D.L.), the. Suzanne Cohn Simon Pancreatic Cancer Research Fund (to S.D.L.), NIH Grant R01 CA204228 (to S.D.L.), NIH Grant P30 CA023108 (to S.D.L.), NIH Grant P30 CA008748, NIH Grant R37 CA244911 (to T.T.), and an NIH/National Cancer Institute Cancer Center Support Grant P30-CA08748 (MSKCC). T.T. is a Rita Allen Foundation, Josie Robertson, and V Foundation Scholar. We thank Dr. Robert Vonderheide for generously providing the KPC4662 cell line. We also thank Dr. Elisa de Stanchina and the Antitumor Core Facility at MSKCC for assistance with drug formulation and in vivo drug administration and the Laboratory of Comparative Pathology at MSKCC for histopathological evaluation of mouse tissues.

1. R. L. Siegel, K. D. Miller, A. Jemal, Cancer statistics, 2019. *CA Cancer J. Clin.* **69**, 7–34 (2019).
2. T. Conroy *et al.*; Groupe Tumeurs Digestives of Unicancer; PRODIGE Intergroup, FOLFIRINOX versus gemcitabine for metastatic pancreatic cancer. *N. Engl. J. Med.* **364**, 1817–1825 (2011).
3. D. D. Von Hoff *et al.*, Increased survival in pancreatic cancer with nab-paclitaxel plus gemcitabine. *N. Engl. J. Med.* **369**, 1691–1703 (2013).
4. B. R. Hall *et al.*, Advanced pancreatic cancer: A meta-analysis of clinical trials over thirty years. *Oncotarget* **9**, 19396–19405 (2018).
5. M. J. Moore *et al.*; National Cancer Institute of Canada Clinical Trials Group, Erlotinib plus gemcitabine compared with gemcitabine alone in patients with advanced pancreatic cancer: A phase III trial of the national cancer Institute of Canada clinical trials group. *J. Clin. Oncol.* **25**, 1960–1966 (2007).
6. N. Niu, L. Wang, In vitro human cell line models to predict clinical response to anticancer drugs. *Pharmacogenomics* **16**, 273–285 (2015).
7. C. P. Day, G. Merlino, T. Van Dyke, Preclinical mouse cancer models: A maze of opportunities and challenges. *Cell* **163**, 39–53 (2015).
8. S. R. Hingorani *et al.*, Trp53R172H and KrasG12D cooperate to promote chromosomal instability and widely metastatic pancreatic ductal adenocarcinoma in mice. *Cancer Cell* **7**, 469–483 (2005).
9. S. R. Hingorani *et al.*, Preinvasive and invasive ductal pancreatic cancer and its early detection in the mouse. *Cancer Cell* **4**, 437–450 (2003).
10. R. Winograd *et al.*, Induction of T-cell immunity overcomes complete resistance to PD-1 and CTLA-4 blockade and improves survival in pancreatic carcinoma. *Cancer Immunol. Res.* **3**, 399–411 (2015).
11. S. Joshi *et al.*, Adapting to stress–Chaperome–C networks in cancer. *Nat. Rev. Cancer* **18**, 562–575 (2018).
12. N. Pillarsetty *et al.*, Paradigms for precision medicinep in epichaperome cancer therapy. *Cancer Cell* **36**, 559–573.e7 (2019).
13. A. Rodina *et al.*, The epichaperome is an integrated chaperome network that facilitates tumour survival. *Nature* **538**, 397–401 (2016).
14. G. Speranza *et al.*, First-in-human study of the epichaperome inhibitor PU-H71: Clinical results and metabolic profile. *Invest. New Drugs* **36**, 230–239 (2018).
15. P. Lito *et al.*, Relief of profound feedback inhibition of mitogenic signaling by RAF inhibitors attenuates their activity in BRAFV600E melanomas. *Cancer Cell* **22**, 668–682 (2012).
16. E. Manchado *et al.*, A combinatorial strategy for treating KRAS-mutant lung cancer. *Nature* **534**, 647–651 (2016).
17. A. D. Basso *et al.*, Akt forms an intracellular complex with heat shock protein 90 (Hsp90) and Cdc37 and is destabilized by inhibitors of Hsp90 function. *J. Biol. Chem.* **277**, 39858–39866 (2002).
18. N. Grammatikakis, J. H. Lin, A. Grammatikakis, P. N. Tsichlis, B. H. Cochran, p50(cdc37) acting in concert with Hsp90 is required for Raf-1 function. *Mol. Cell. Biol.* **19**, 1661–1672 (1999).
19. K. L. Bryant *et al.*, Combination of ERK and autophagy inhibition as a treatment approach for pancreatic cancer. *Nat. Med.* **25**, 628–640 (2019).
20. T. C. Chou, Drug combination studies and their synergy quantification using the Chou-Talalay method. *Cancer Res.* **70**, 440–446 (2010).
21. A. Sinha *et al.*, Mesenchymal-like pancreatic cancer cells harbor specific genomic alterations more frequently than their epithelial-like counterparts. *Mol. Oncol.* **8**, 1253–1265 (2014).
22. M. Ghandi *et al.*, Next-generation characterization of the cancer cell line encyclopedia. *Nature* **569**, 503–508 (2019).
23. S. F. Boj *et al.*, Organoid models of human and mouse ductal pancreatic cancer. *Cell* **160**, 324–338 (2015).
24. S. I. Choi *et al.*, Development of patient-derived preclinical platform for metastatic pancreatic cancer: PDOX and a subsequent organoid model system using percutaneous biopsy samples. *Front. Oncol.* **9**, 875 (2019).
25. H. Tiriac *et al.*, Organoid profiling identifies common responders to chemotherapy in pancreatic cancer. *Cancer Discov.* **8**, 1112–1129 (2018).
26. G. J. Yoshida, Applications of patient-derived tumor xenograft models and tumor organoids. *J. Hematol. Oncol.* **13**, 4 (2020).
27. S. E. Gould, M. R. Junttila, F. J. de Sauvage, Translational value of mouse models in oncology drug development. *Nat. Med.* **21**, 431–439 (2015).
28. A. Neesse *et al.*, Stromal biology and therapy in pancreatic cancer. *Gut* **60**, 861–868 (2011).
29. I. M. Stromnes, K. E. DelGiorno, P. D. Greenberg, S. R. Hingorani, Stromal reengineering to treat pancreas cancer. *Carcinogenesis* **35**, 1451–1460 (2014).
30. A. M. Waters, C. J. Der, KRAS: The critical driver and therapeutic target for pancreatic cancer. *Cold Spring Harb. Perspect. Med.* **8**, a031435 (2018).
31. A. A. Samatar, P. I. Poulikakos, Targeting RAS-ERK signalling in cancer: Promises and challenges. *Nat. Rev. Drug Discov.* **13**, 928–942 (2014).
32. K. T. Flaherty *et al.*; METRIC Study Group, Improved survival with MEK inhibition in BRAF-mutated melanoma. *N. Engl. J. Med.* **367**, 107–114 (2012).
33. K. B. Kim *et al.*, Phase II study of the MEK1/MEK2 inhibitor Trametinib in patients with metastatic BRAF-mutant cutaneous melanoma previously treated with or without a BRAF inhibitor. *J. Clin. Oncol.* **31**, 482–489 (2013).
34. A. B. Turke *et al.*, MEK inhibition leads to PI3K/AKT activation by relieving a negative feedback on ERBB receptors. *Cancer Res.* **72**, 3228–3237 (2012).
35. T. K. Hayes *et al.*, Long-term ERK inhibition in KRAS-mutant pancreatic cancer is associated with MYC degradation and senescence-like growth suppression. *Cancer Cell* **29**, 75–89 (2016).
36. A. V. Vaseva *et al.*, KRAS suppression-induced degradation of MYC is antagonized by a MEK5-ERK5 compensatory mechanism. *Cancer Cell* **34**, 807–822.e7. (2018).
37. W. B. Pratt, The hsp90-based chaperone system: Involvement in signal transduction from a variety of hormone and growth factor receptors. *Proc. Soc. Exp. Biol. Med.* **217**, 420–434 (1998).
38. G. P. Nagaraju *et al.*, Inhibition of HSP90 overcomes resistance to chemotherapy and radiotherapy in pancreatic cancer. *Int. J. Cancer* **145**, 1529–1537 (2019).
39. L. Giulino-Roth *et al.*, Inhibition of Hsp90 suppresses PI3K/AKT/mTOR signaling and has antitumor activity in burkitt lymphoma. *Mol. Cancer Ther.* **16**, 1779–1790 (2017).
40. G. Ohji *et al.*, Suppression of the mTOR-raptor signaling pathway by the inhibitor of heat shock protein 90 geldanamycin. *J. Biochem.* **139**, 129–135 (2006).
41. E. A. Collisson *et al.*, A central role for RAF→MEK→ERK signaling in the genesis of pancreatic ductal adenocarcinoma. *Cancer Discov.* **2**, 685–693 (2012).
42. R. A. Evans *et al.*, Lack of immunoediting in murine pancreatic cancer reversed with neoantigen. *JCI Insight* **1**, 88328 (2016).
43. K. P. Olive *et al.*, Inhibition of Hedgehog signaling enhances delivery of chemotherapy in a mouse model of pancreatic cancer. *Science* **324**, 1457–1461 (2009).